Stability Analysis of a Synchronous Generator-Based Control Technique used in Large-Scale Grid Integration of Renewable Energy

Majid Mehrasa
C-MAST/UBI
Portugal

Amir Sepehr, Edris Pouresmaeil, Jorma Kyyrä
Dep. of Elec. Eng. and Auto.,
Aalto University,
Finland

Mousa Marzband
Dep. of Mech. and Elec. Eng. Northumbria University,
UK

João P. S. Catalão
INESC TEC and FEUP, Porto,
C-MAST/UBI, Covilha, and
INESC-ID/IST-UL, Lisbon,
Portugal

***Abstract*—A synchronous generator (SG)-based control technique is proposed in this paper to force the grid voltage magnitude and frequency to follow the desired values under high penetration of renewable energy sources. A more detailed relationship between power dynamic model and SGs characteristics has been considered in the proposed control strategy. The active and reactive power error-based curve of the proposed control technique is evaluated in detail. Besides, the grid angular frequency error based on the proposed control technique performance is assessed in the next step. Simulation is employed in Matlab/Simulink to verify the operation of the proposed control technique in power converters for large-scale integration of renewable energy sources into the power grids.**

Keywords—Renewables integration, double synchronous controller, power grid stability, virtual inertia, mechanical power.

I. INTRODUCTION

Integrating the large-scale renewable energy resources (RERs) into the power grid offers several benefits i.e., economic and environmental benefits [1]-[2].

In the meantime, it also increases different technical challenges regarding the grid stability and reliability due to the high variability, unpredictable fluctuation and intermittent characteristics of these sources [3]. Generally, RERs are connected to the power grid via power electronics converters [4], which the lack of inertia in these converter-based power generators can increase their negative impacts on the power grid stability. These impacts may also be consisted of their peculiar transient dynamics behavior and are the opposite of the operation of synchronous generators.

Consequently, the operation of converter-based generators should be controlled with some specific functionalities based on inherent characteristics of synchronous generators; thus, successfully reaching their high penetration level in power grid [5].

Therefore, designing an appropriate control technique for grid-interfaced converters to deal with the stability issues of the power grid has been regarded as one of the main tasks for scientists in power and energy societies [6]-[7].

Edris Pouresmaeil acknowledges the support by the Department of Electrical Engineering and Automation at Aalto University, Finland. Moreover, João P. S. Catalão acknowledges the support by FEDER funds through COMPETE 2020 and by Portuguese funds through FCT, under Projects SAICT-PAC/0004/2015 - POCI-01-0145-FEDER-016434, POCI-01-0145-FEDER-006961, UID/EEA/50014/2013, UID/CEC/50021/2013, UID/EMS/00151/2013, and 02/SAICT/2017 - POCI-01-0145-FEDER-029803, and also funding from the EU 7th Framework Programme FP7/2007-2013 under GA no. 309048.

Various control aims such as accurate power sharing and grid voltage regulation have been considered in a large-scale integration of microgrid or multi-distributed generations (DG) connections for achieving a stable performance [8]-[9].

In addition, along with increasing the challenges of high penetration of RERs into the power grid [10]-[11], several control strategies have focused on improving the stability of grid frequency and voltage magnitude.

For this reason, several studies have been reported in the literature regarding the emulation of synchronous generator characteristics by power converters [12]- [16].

Reference [12] has presented a complete review associated with the main concepts of virtual synchronous generators and their ability at controlling the power grid under the high level of DGs penetration. A coordinated control-based energy storage system combined with virtual synchronous generators has been proposed in [13] to provide emulation of the synchronous generator for power converters. In [14], using a non-ideal proportional-resonant (PR) controller and SG features embedded in swing equation, a synchronous active proportional resonant-based control strategy has been proposed to control a grid-interfaced converter for high penetration of RERs into the power grid. Numerical simulations have been used in [15] to illustrate a specific virtual synchronous machine-based concept along with its related mathematical for controlling power converters in smart grid application. Reference [16] has proposed a power-based control technique to force the interfaced power converter to have the inherent features of synchronous power generators by injecting both active and reactive power into the power grid. More references in [17]-[19] have assessed the synchronous generators-based control techniques and their operation in various operating conditions.

This paper presents a new control strategy based on synchronous generator features that provides a stable operating condition for the grid under high penetration of renewable energy resources. Then, a comprehensive stability analysis based on the active and reactive power error curve is presented. The grid angular frequency variations are also assessed. Simulation results show the ability of the proposed control technique for grid-interfaced converters to guarantee the stability of the power grid under high penetration of renewable energy sources.

978-1-5386-5326-5/18/$31.00 ©2018 IEEE

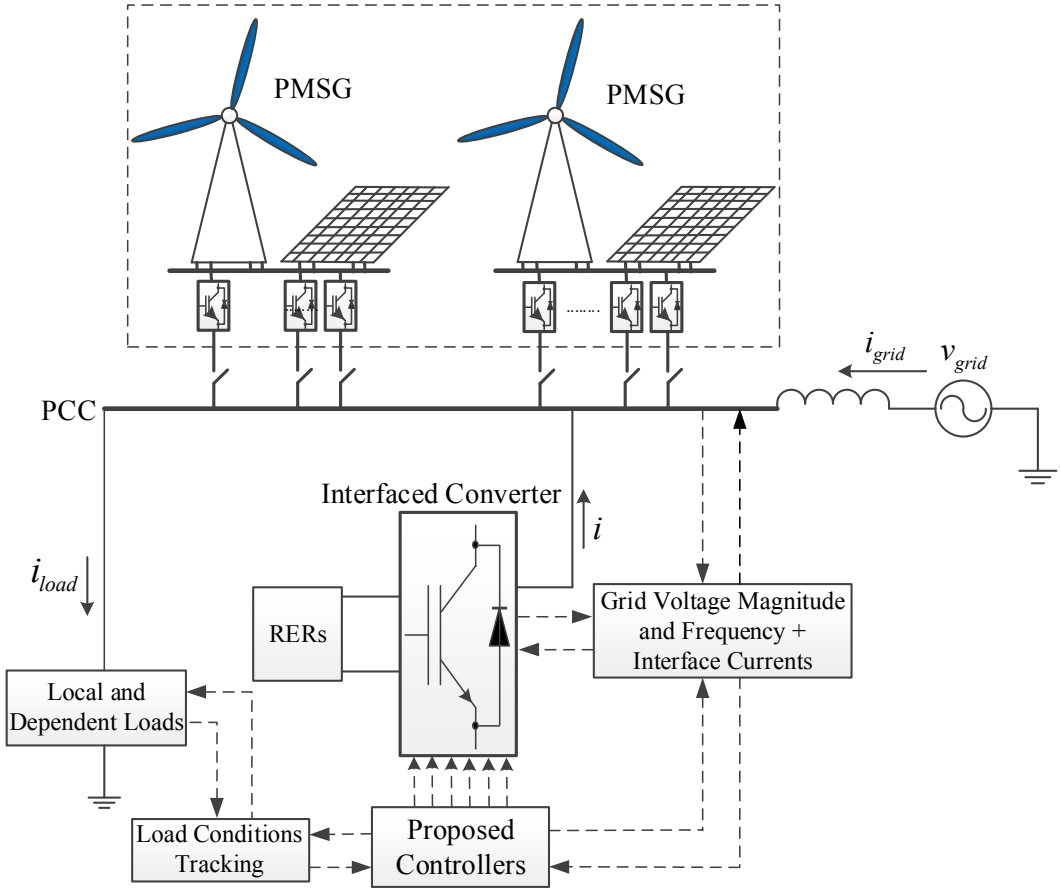

Fig. 1. An illustrative diagram corresponding to system structure/topology employed in the study.

II. PROPOSED CONTROL TECHNIQUE

Systems and dynamics are usually modeled by mathematical representation. The mathematical models or system models usually are able to represent the operating conditions of real systems. Considering the interfaced converter in Fig. 1, the dynamic model of the interfaced converter based on the d-q components of its currents can be driven as given in Eq. (1).

$$\frac{d}{dt}\begin{bmatrix} Li_d \\ Li_q \\ Cv_{dc} \end{bmatrix} = \begin{bmatrix} -R & \omega L & u_d \\ -\omega L & -R & u_q \\ -u_d & -u_q & 0 \end{bmatrix}\begin{bmatrix} i_d \\ i_q \\ v_{dc} \end{bmatrix} + \begin{bmatrix} -v_d \\ -v_q \\ -i_{dc} \end{bmatrix} \tag{1}$$

where L, R, ω are the inductance, resistance, and angular frequency of the interfaced converter, respectively. i_{dq}, v_{dq} and u_{dq} are the output currents, output voltages, and switching state functions of the interfaced converter in d-q reference frame, respectively. v_{dc}, i_{dc} and C are the dc –link voltage, dc-link current, and the capacitance of dc-link voltage, respectively. By assuming the converter active and reactive power as $P=i_d v_d$ and $Q=-i_q v_d$, (1) can be rewritten as:

$$\frac{d}{dt}\begin{bmatrix} \frac{L}{R}P \\ \frac{L}{R}Q \\ RCP_{c1} \end{bmatrix} = \begin{bmatrix} -1 & -\frac{\omega L}{R} & u_d \\ \frac{\omega L}{R} & -1 & -u_q \\ -u_d & u_q & 0 \end{bmatrix}\begin{bmatrix} P \\ Q \\ P_{c1} \end{bmatrix} + \begin{bmatrix} -P_{pd} \\ P_{pdq} \\ -P_{c2} \end{bmatrix} \tag{2}$$

where, $P_{c1}=v_{dc}v_d/R$, $P_{c2}=i_{dc}v_d$, $P_{pd}=v_d^2/R$, and $P_{pdq}=v_d v_q/R$. By transforming (2) into the frequency domain, (3) can be achieved as:

$$\begin{bmatrix} (\frac{L}{R}s+1) & \frac{\omega L}{R} & -u_d \\ -\frac{\omega L}{R} & (\frac{L}{R}s+1) & u_q \\ u_d & -u_q & RCs \end{bmatrix}\begin{bmatrix} P \\ Q \\ P_{c1} \end{bmatrix} + \begin{bmatrix} P_{pd} \\ -P_{pdq} \\ P_{c2} \end{bmatrix} = 0 \tag{3}$$

The relation between the electrical and mechanical parts of a synchronous generator can be stated by the following swing equation as:

$$J\frac{d\omega}{dt} = \frac{P_m - P}{\omega} \tag{4}$$

where J and P_m are the moment inertia and mechanical power of synchronous generator, respectively. By applying the small signal linearization to (4), the error of angular frequency can be calculated as:

$$\Delta\omega = \frac{1}{\omega^* J}\cdot\frac{\Delta P_m - \Delta P}{s + \left(P_m^* - P^*\right)/\omega^{*2} J} \tag{5}$$

where P_m^*, P^*, and ω^* are the reference values of active power, mechanical power, and angular frequency, respectively.

By a control-based description of the active power error, the following equation can be achieved as:

$$\frac{\Delta P}{s}=\frac{\Delta P_m}{s}-\left(\omega^* J+\frac{\left(P_m^*-P^*\right)}{\omega^* s}\right)\Delta\omega \tag{6}$$

Assuming a constant power for the interfaced converter with relationship of $P^2+Q^2=constant$ and using small signal linearization, gives:

$$\frac{\Delta Q}{s}=-\frac{P^*}{Q^*}\frac{\Delta P_m}{s}+\frac{P^*}{Q^*}\left(\omega^* J+\frac{\left(P_m^*-P^*\right)}{\omega^* s}\right)\Delta\omega \tag{7}$$

where Q^* is the reference value of reactive power. Using (5)-(7), the dynamic model of the interfaced converter based on characteristics of SG is given as:

$$\frac{1}{s}\begin{bmatrix}\Delta\omega\\ \Delta P\\ \Delta Q\end{bmatrix}=\begin{bmatrix}0 & \dfrac{-1/\omega^* Js}{s+\left(P_m^*-P^*\right)/\omega^{*2}J} & 0\\ -\left(\omega^* J+\dfrac{\left(P_m^*-P^*\right)}{\omega^* s}\right) & 0 & 0\\ \dfrac{P^*}{Q^*}\left(\omega^* J+\dfrac{\left(P_m^*-P^*\right)}{\omega^* s}\right) & 0 & 0\end{bmatrix}\times\begin{bmatrix}\Delta\omega\\ \Delta P\\ \Delta Q\end{bmatrix}+\begin{bmatrix}\dfrac{1}{\omega^* Js}\cdot\dfrac{1}{s+\left(P_m^*-P^*\right)/\omega^{*2}J}\\ \dfrac{1}{s}\\ -\dfrac{P^*}{Q^*}\dfrac{1}{s}\end{bmatrix}\Delta P_m \tag{8}$$

Based on Fig.2, both components of proposed control technique are consisted of several closed loops achieved by SGs features and inherent dynamic model of interfaced converter. According to Fig.2, all SGs features included virtual inertia and mechanical power error can be seen in proposed controller.

III. EVALUATION OF THE ACTIVE AND REACTIVE POWER ERROR-BASED CURVE

By applying small-signal linearization to two first terms of (2), equations (9) and (10) can be achieved as:

$$\frac{L}{R}s\Delta P+\Delta P+\frac{\Delta\omega L}{R}Q^*+\frac{\omega^* L}{R}\Delta Q-\Delta u_d P_{c1}^*-u_d^*\Delta P_{c1}+\Delta P_d=0 \tag{9}$$

$$\frac{L}{R}s\Delta Q+\Delta Q-\frac{\Delta\omega L}{R}P^*-\frac{\omega^* L}{R}\Delta P+\Delta u_q P_{c1}^*+u_q^*\Delta P_{c1}-\Delta P_{dq}=0 \tag{10}$$

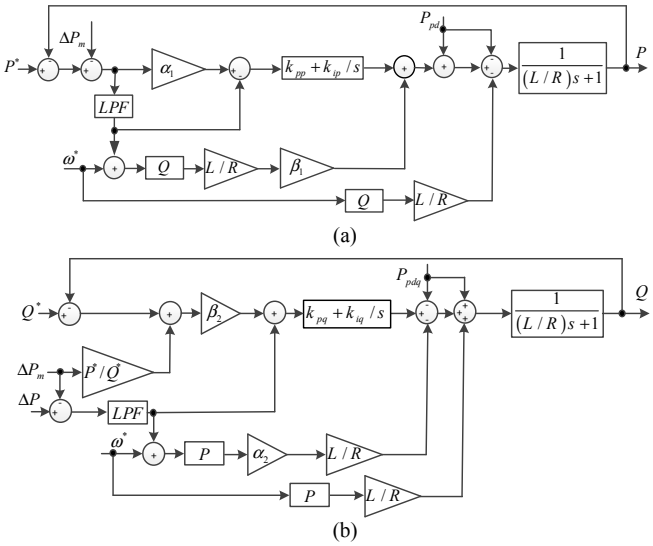

Fig. 2. The proposed control technique based on inherit feature of synchronous generator.

where u^*_{dq} and P^*_{c1} are the reference values of switching functions and P_{c1}, respectively. And also combining (6), (7), (9) and (10), the error curve for the DSC's active and reactive power can be achieved as (11):

$$\left(\Delta P+a_{DSC}\right)^2+\left(\Delta Q+b_{DSC}\right)^2=R_{DSC}^2 \tag{11}$$

where ($-a_{DSC}$,$-b_{DSC}$) and R_{DSC} are the radius and center parameters, respectively. The radius and center parameters of the active and reactive power error curve are specified as:

$$R_{DSC}=\sqrt{\left(\frac{\left(P_m^*-P^*\right)LQ^*\Delta\omega-\omega^* LQ^*\Delta P_m-R\omega^{*2}J\Delta\omega Q^*-\omega^{*3}JP^* L\Delta\omega}{2\omega^* LQ^*}\right)^2+\left(\frac{L\omega^* P^*\Delta P_m-\omega^{*3}J\Delta\omega LQ^*-LP^*\left(P_m^*-P^*\right)\Delta\omega+\omega^{*2}JP^* R\Delta\omega}{2LQ^*\omega^*}\right)^2+\frac{\left(\begin{array}{l}\omega^* JLQ^{*2}\Delta\omega^2-\omega^* JP_{c1}^* Q^* R\Delta u_d\Delta\omega-\omega^* JQ^* Ru_d^*\Delta P_{c1}\Delta\omega\\ +\omega^* JQ^* R\Delta P_d\Delta\omega+\omega^* JP^{*2}L\Delta\omega^2\\ -\omega^* JP^* RP_{c1}^*\Delta u_q\Delta\omega-\omega^* JP^* Ru_q^*\Delta P_{c1}\Delta\omega+\omega^* JP^* R\Delta P_{dq}\Delta\omega\end{array}\right)}{Q^* L}}$$

$$a_{DSC}=\left(\frac{\left(P_m^*-P^*\right)LQ^*\Delta\omega-\omega^* LQ^*\Delta P_m-R\omega^{*2}J\Delta\omega Q^*-\omega^{*3}JP^* L\Delta\omega}{2\omega^* LQ^*}\right)$$

$$b_{DSC}=\left(\frac{L\omega^* P^*\Delta P_m-\omega^{*3}J\Delta\omega LQ^*-LP^*\left(P_m^*-P^*\right)\Delta\omega+\omega^{*2}JP^* R\Delta\omega}{2LQ^*\omega^*}\right)$$

The virtual mechanical power error alterations can impact on the active and reactive power error curve of the proposed control-based interfaced converter according to Fig. 3.

As it is expected, increasing virtual mechanical power error leads to the larger error curve, which shows the importance of virtual mechanical power error in the operation of proposed control technique. These increased errors will lead to instability for power grid.

Choosing different values for the virtual inertia can cause the error curve to be changed based on Fig. 4. According to this figure, the critical case is associated with very high value of the virtual inertia that generates the largest error curve along with instability behavior of power grid. By considering the low-high values of the virtual inertia, the best response is achieved. But, selecting very low values for the virtual inertia can lead to larger curve but not as the same that is obtained for very high virtual inertia, as illustrated in Fig. 4.

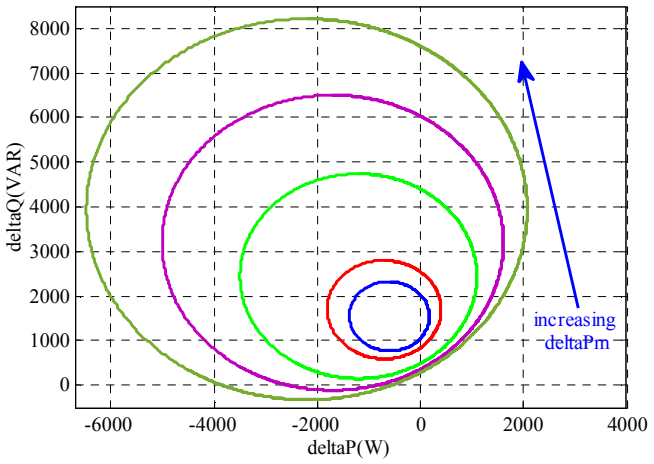

Fig.3. The effects of increasing ΔP_m on the DSC error curve.

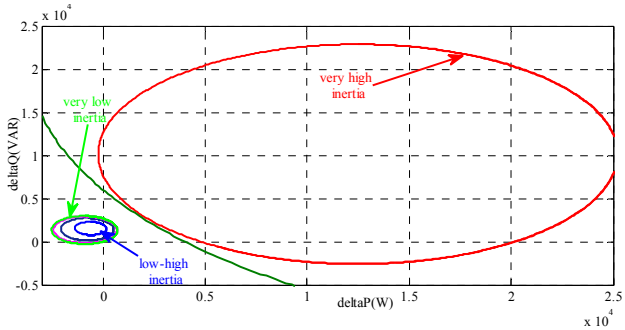

Fig. 4. The effects of changing the virtual inertia (J) on the DSC error curve.

It can be understood from Fig. 4, the virtual inertia of the proposed synchronous generator-based control strategy plays a key role at reaching the decreased values for both active and reactive power errors.

IV. Assessment of the Grid Frequency Variations

The small signal method is applied to the first term of (2) and subsequently (12) can be obtained as:

$$\left(\frac{L}{R}s+1\right)\Delta P+\frac{\Delta\omega L}{R}Q^{*}+\frac{\omega^{*}L}{R}\Delta Q \qquad (12)$$
$$-\Delta u_d P_{c1}^{*}-u_d^{*}\Delta P_{c1}+\Delta P_d=0$$

By achieving ΔP from (6) and substituting the result into (12), variations of the grid frequency can be achieved as:

$$\Delta\omega=F_{P_m}\Delta P_m+F_Q\Delta Q+F_{u_d}\Delta u_d+F_{P_{c1}}\Delta P_{c1}+F_{P_d}\Delta P_d \qquad (13)$$

$$F_{P_m}=\frac{\left(\frac{L}{R}s+1\right)}{\Delta_\omega},F_Q=\frac{\frac{\omega^{*}L}{R}}{\Delta_\omega},F_{u_d}=-\frac{P_{c1}^{*}}{\Delta_\omega},$$

$$F_{P_{c1}}=-\frac{u_d^{*}}{\Delta_\omega},F_{P_d}=\frac{1}{\Delta_\omega} \qquad (14)$$

$$\Delta_\omega=\left(\frac{\omega^{*}JL}{R}s^{2}+\left[\left(\frac{\left(P_m^{*}-P^{*}\right)L}{R\omega^{*}}\right)+\omega^{*}J\right]s+\left[\left(P_m^{*}-P^{*}\right)/\omega^{*}+\frac{Q^{*}L}{R}\right]\right)$$

Based on (13), the effects of each component are considered to evaluate the responses of the grid angular frequency versus the varied values of virtual inertia. As can be seen from (13) and (14), the transfer function relating to the virtual mechanical power error is different from other components errors. For three virtual inertia values of $J_3>J_2>J_1$, the Nyquist diagrams of transfer functions around the operating angular frequency associated with the virtual mechanical power error and other errors are drawn in Fig. 5. Based on Figs. 5(a) and (b), it can be explained that increasing the virtual inertia leads to better response for the grid angular frequency error under the presence of various error components. In fact, increasing the virtual inertia can help the proposed controller to reach a grid frequency near to its reference value with almost zero error.

V. Results and Discussions

In this section, the ability of the synchronous generator-based control technique is assessed based on regulating the grid frequency and voltage magnitude at their desired values.

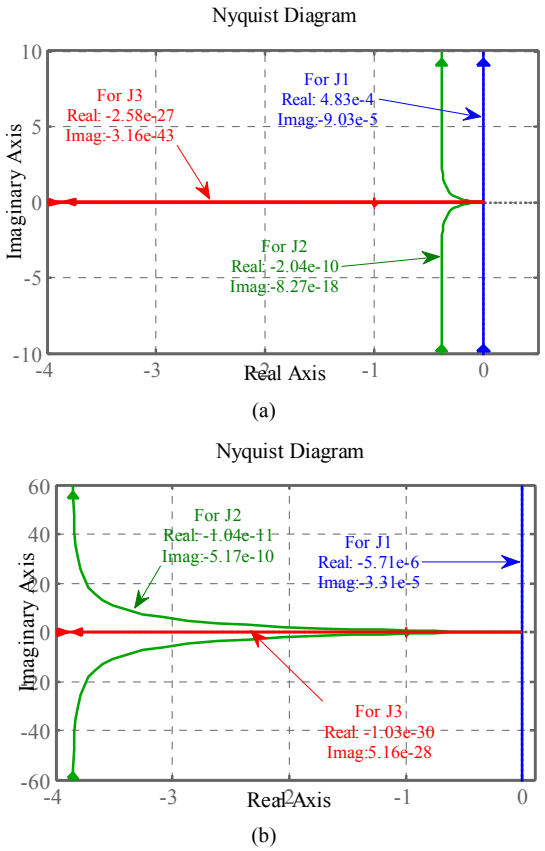

Fig. 5. The Nyquist diagram of Δω versus the step variation of: (a) VMPE (ΔPm), and (b) other components errors of (ΔQ, Δud, ΔPc1, and ΔPd).

To accurately analysis this ability, an abrupt disconnection of renewable energy resources from power grid happens at t=0.1s. The simulations are performed in MATLAB/SIMULINK software and the system parameters are given in Table I.

A. Grid frequency and voltage magnitude evaluation

The operation of the proposed control technique can be affected by various values of the virtual inertia. To deal with power grid stability through performance of the proposed control strategy, the acceptable region of the inertia values is assessed in this sub-section.

According to Fig.6(a), the grid frequency will be noticeably deteriorated for both very low and very high values of inertia. Low-high value of inertia is the best option for reaching the stable response of grid frequency.

TABLE I: Simulation Parameters

Parameter	Value	Parameter	Value
dc-link Voltage (v_{dc})	850 V	J	1e3 kg.m^2
Phase ac voltage	220 V	P_m	3.3 kW
Fundamental frequency	50 Hz	P	3 kW
Switching frequency	10 kHz	Q	2 kVAr
Interface converter resistance	0.1 Ohm	Interface converter	45 mH

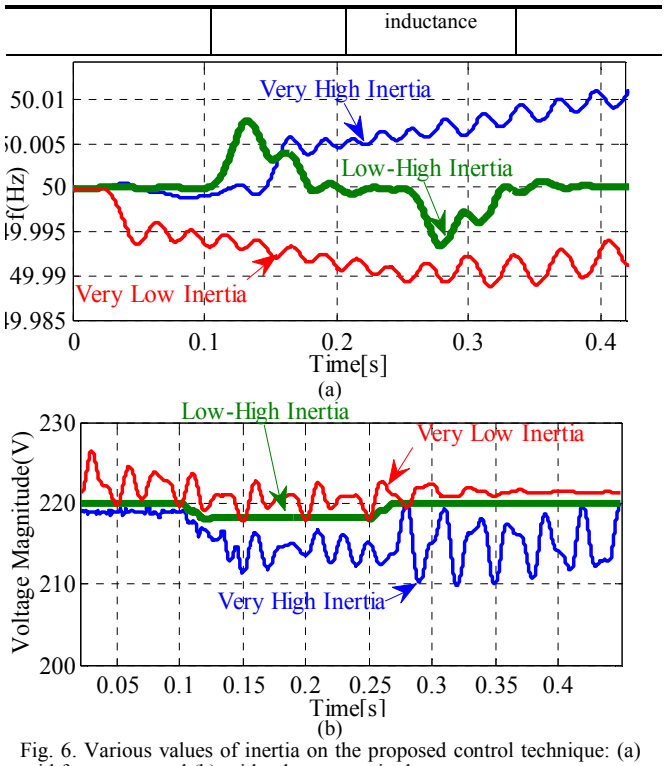

Fig. 6. Various values of inertia on the proposed control technique: (a) grid frequency, and (b) grid voltage magnitude.

On the other hand, with very low inertia, the grid voltage magnitude can hardly move on the upper path of its desired value with high fluctuations. But, choosing a very high value of the inertia leads to an uncontrollable behavior from the grid voltage magnitude with severe fluctuations as depicted in Fig. 6(b).

Similar to grid frequency, the best response for grid voltage magnitude is achieved by low-high value of inertia.

VI. CONCLUSION

A control technique based on inherent features of synchronous generators as well as the power-based dynamic model of interfaced converters has been introduced in this paper. All effects of the virtual inertia and mechanical power error upon the active and reactive power error have been assessed completely by the use of a power error-based curve. Moreover, the grid angular frequency alterations have been investigated. The operation of the proposed control technique has been evaluated by simulation results through Matlab/Simulink. The obtained results confirmed the accurate performance of the proposed control technique for grid-interfaced converters to guarantee a stable operating condition for the power grid under high penetration of renewable energy sources.

REFERENCES

[1] H. Lund and B. V. Mathiesen, ‘‘Energy system analysis of 100% renewable energy systems—The case of Denmark in years 2030 and 2050,’’ *Energy*, vol. 34, no. 5, pp. 524–531, May 2009.

[2] E. Pouresmaeil, H.R. Shaker, M. Mehrasa, M.A. Shokridehaki, E.M.G. Rodrigues, and J.P.S Catalão, “Integration of renewable energy for the harmonic current and reactive power compensation,’’ *POWERENG,* Sep. 2015.

[3] M. Mehrasa, E. Pouresmaeil, B.N. Jørgensen, and J.P.S Catalão, “A control plan for the stable operation of microgrids during grid-connected and islanded modes,’’ *Electric Power Systems Research*, vol. 129, pp. 10-22, Dec. 2015.

[4] A. Trivedi, M. Singh, “Repetitive Controller for VSIs in Droop-Based AC-Microgrid,’’ *IEEE Transactions on Power Electronics* 2017; 32 (8): 6595 – 6604.

[5] E. Pouresmaeil, H. R. Shaker, M. Mehrasa, M.A. Shokridehaki, E. M.G. Rodrigues, J.P.S. Catalão, “Stability analysis for operation of DG units in smart grids,’’ POWERENG, Sep. 2015.

[6] V. Nasirian, Q. Shafiee, JM. Guerrero, FL. Lewis, A. Davoudi, “Droop-Free Distributed Control for AC Microgrids,’’ *IEEE Transactions on Power Electronics* 2016; 31 (2): 1600 – 1617.

[7] M. Mehrasa, M. Rezanejhad, E. Pouresmaeil, J.P.S. Catalão, S. Zabihi, “Analysis and control of single-phase converters for integration of small-scaled renewable energy sources into the power grid,’’ 7th *Power Electronics and Drive Systems Technologies Conference* (PEDSTC), 384-389, Sep. 2016.

[8] V. Karapanos, P. Kotsampopoulos, N. Hatziargyriou, “Performance of the linear and binary algorithm of virtual synchronous generators for the emulation of rotational inertia,’’ *Electric Power Systems Research* 2015; 123: 119-127.

[9] L. Yang, J. Wang, Y. Ma, J. Wang, X. Zhang, LM. Tolbert, FF. Wang, K. Tomsovic, “Three-Phase Power Converter-Based Real-Time Synchronous Generator Emulation,’’ *IEEE Transactions on Power Electronics* 2017; 32 (2): 1651 – 1665.

[10] P.M.R. Almeida, F.J. Soares, J.A.P. Lopes, “Electric vehicles contribution for frequency control with inertial emulation,’’ *Electric Power Systems Research* 2015; 127: 141-150.

[11] M Guan, W Pan, J Zhang, Q Hao, J Cheng, X Zheng, “Synchronous Generator Emulation Control Strategy for Voltage Source Converter (VSC) Stations,’’ *IEEE Transactions on Power Systems* 2015; 30 (6): 3093 – 3101.

[12] H Bevrani, T Ise, Y Miura, “Virtual synchronous generators: A survey and new perspectives,’’ *International Journal of Electrical Power & Energy Systems* 2014; 54: 244-254.

[13] J Fang, Y Tang, H Li, X Li, “A Battery/Ultracapacitor Hybrid Energy Storage System for Implementing the Power Management of Virtual Synchronous Generators,’’ *IEEE Transactions on Power Electronics* 2018; 33 (4); 2820 – 2824.

[14] M. Mehrasa, R. Godina, E. Pouresmaeil, I. Vechiu, R. L. Rodríguez, J. P. S. Catalão, ‘‘Synchronous active proportional resonant-based control technique for high penetration of distributed generation units into power grids,’’ *Innovative Smart Grid Technologies Conference Europe* (ISGT-Europe), 2017 IEEE PES, pp. 1-6, January 2018.

[15] S. D’Arco, JA. Suul, OB. Fosso, “A Virtual Synchronous Machine implementation for distributed control of power converters in Smart Grids,’’ *Electric Power Systems Research* 2015, vol. 122: pp. 180-197, May 2015.

[16] E. Pouresmaeil, M. Mehrasa, R. Godina, I. Vechiu, R. L. Rodríguez, J.P.S. Catalão, ‘‘Double synchronous controller for integration of large-scale renewable energy sources into a low-inertia power grid,’’ *Innovative Smart Grid Technologies Conference Europe* (ISGT-Europe), 2017 IEEE PES, pp. 1-6, January 2018.

[17] E. Pouresmaeil, M. Mehrasa, R. Godina, I. Vechiu, R. L. Rodríguez, J.P.S. Catalão, ‘‘Double synchronous controller for integration of large-scale renewable energy sources into a low-inertia power grid,’’ *Innovative Smart Grid Technologies Conference Europe* (ISGT-Europe), 2017 IEEE PES, pp. 1-6, January 2018.

[18] MA. Torres, LA. Lopes, LA. Moran, and JR. Espinoza, “Self-tuning virtual synchronous machine: A control strategy for energy storage systems to support dynamic frequency control,” *IEEE Trans. Energy Convers*., vol. 29, no. 4, pp. 833–840, Dec 2014.

[19] SD. Arco and JA. Suul, “Equivalence of virtual synchronous machines and frequency-droops for converter-based microgrids,” IEEE Trans. Smart Grid, vol. 5, no. 1, pp. 394–395, Jan. 2014.